THE FRACTOGRAPHY OF FATIGUE CRACKING IN A CAST ALUMINIUM ALLOY AT A RANGE OF TEMPERATURES.

L.E. CULVER, J.C. BALTHAZAR and J.C. RADON*

Fatigue crack threshold and growth under fluctuating tension loads have been examined in the cast aluminium alloy BS1490-LM30. Compact specimens were used for tensile fatigue crack propagation tests at 50 Hz and threshold stress-intensity ranges, ΔK_{th}, of about 4.3 $MN/m^{3/2}$ and 2.9 $MN/m^{3/2}$ were found at a stress ratio of 0.08 for temperatures of 20° and 250 °C respectively. A fractographic study of the broken specimens was conducted over the whole fatigue cracked zone and revealed a mixed mode of fracture consisting of cleavage silicon precipitate and ductile tearing of the aluminium matrix.

INTRODUCTION

Fracture Mechanics concepts have been extensively applied to explain fatigue behaviour in metals but most work in aluminium alloys has concentrated on wrought materials and in spite of their increasing use in industry little attention has been paid to aluminium alloys in the cast condition. Striation formation is generally accepted as the predominant mechanism of fatigue crack propagation [1,2], the formation of these striations being related to the intensive plastic deformation taking place around the crack during each load cycle. However, recent evidence has shown that fatigue cracking can involve much more complicated processes. GERBERICH and MOODY [3] for instance have identified at least ten microscopic fracture modes of fatigue crack propagation as alternatives to ductile striations, whilst McEVILY [4] and BEEVERS [5] have also shown that fatigue cracking is strongly dependent on stress intensity, microstructure, environment and other factors. In the present work an investigation was carried out using a cast hypereutectic aluminium-silicon alloy which has recently been in use in the automotive industry. Compact specimens were tested under fluctuating tension loads at different temperatures and a fractographic study of the broken specimens was conducted over the entire fatigue cracked surface.

* Department of Mechanical Engineering, Imperial College - London.

EXPERIMENTAL PROCEDURE

Material

The material used in the present work was LM-30 a high-silicon content aluminium alloy having excellent casting properties, wear resistance comparable to cast iron and low weight. Originally it was designed specifically for automobile pressure die cast cylinder blocks operating without cylinder liners but it may also be used for a range of applications where high wear resistance associated with lightness is required. LM-30 is chemically similar to the American alloys 390 and A 390 [6] as may be seen from their respective compositions given in table 1.

TABLE 1 - CHEMICAL COMPOSITION

%	LM-30	390	A390
Si	16.0 -18.0	16.0 -18.0	16.0 - 18.0
Cu	4.0 - 5.0	4.0 - 5.0	4.0 - 5.0
Fe	1.1	0.6 - 1.1	0.5 max
Mg	0.4 - 0.7	0.45 - 0.65	0.45 - 0.65
Mn	0.3	0.1 max	0.1 max
Zn	0.2	0.1 max	0.1 max
Ti	0.2	0.2 max	0.2 max
Ni,Pb,Sn	0.1 each		
Others		0.1 max each 0.2 max tot	0.1 max each 0.2 max tot
Al	balance	balance	balance

Metallographic analysis shows that the microstructure, Figure 1, basically contains approximately 6% of primary silicon embedded in a eutectic matrix which contains 99.8% of aluminium. Without prior refinement these primary silicon crystals grow comparatively large and irregular in shape thus decreasing the tensile properties [7].

Typical LM-30 mechanical properties, Table 2, show that hardness, tensile and yield properties are comparable with other common casting aluminium alloys. The ductility of LM-30 is very low, but this is not considered a disadvantage as most of its potential applications are as a replacement for cast irons.

TABLE 2 - TYPICAL MECHANICAL PROPERTIES

ALLOY CONDITION	CASTING METHOD	UTS MPa	YS MPa	ELONG.	HARD.	END. LIMIT MPa
LM-30 M	Die	210	190	<1	120*	100
390 F	Die	279	241	1**	120 BHN	135
390 T5	Die	296	265	1**		
A390 F	P.Mold	200	200	1**	110 BHN	
	Sand	179	179	1**	110 BHN	
A390 T5	P.Mold	200	200	1**	110 BHN	
	Sand	179	179	1**	100 BHN	

* - Vickers - 2.5 Kgf load ** - 2" G.L.
M and F = As cast, TS = Stress relieved only, T5 = Aged 8hr,232 °C

Specimen and Test Procedures.

The fatigue crack propagation tests were made on ASTM type compact specimens, Figure 2, as established by the ASTM Test Method E 647-81 for Constant-Load-Amplitude fatigue crack growth rates above 10^{-8} m/cycle. The specimens were 25 mm thick and were cycled in uniaxial tension in a DOWTY electro-hydraulic fatigue test machine at a stress-intensity ratio R ($R=K_{min}/K_{max}$) of 0.08 and at temperatures of 20 °C and 250 °C. A specially constructed DONALDSON furnace was used for the tests at high temperature with the temperature kept constant within ± 2 °C by a HONEYWELL temperature controller. A sinusoidal load wave form was applied to all specimens at a test frequency of 50 Hz. A load cell of maximum capacity 15 kN was used and the crack length was measured by a travelling microscope with an accuracy of 0.02 mm.

The test data, crack length versus elapsed cycles, were processed by the secant method to obtain the fatigue crack growth rate da/dN as a function of the corresponding stress-intensity factor range ΔK_1. The value of ΔK_1 was calculated using the expression:

$$\Delta K_1 = \frac{\Delta P}{BW^{1/2}} f(a/W) \qquad (1)$$

where B is the thickness of the specimen, W the distance between the load axis and the far edge of the specimen and a is the crack length. The geometric factor f(a/W) was calculated from a polynomial expression given by SAXENA and HUDDAK [8]:

$$f(a/W) = \frac{2+a/W}{(1+a/W)^{3/2}}\left[0.866 + 4.64(a/w) - 13.32(a/W)^2 + 14.72(a/W)^3 - 5.6(a/W)^4\right] \qquad (2)$$

which is valid for $0.2<(a/W)<0.95$.

The results, ΔK_1 versus da/dN, were plotted in the usual way, Figure 3.

Fractographic Analysis.

The fracture surfaces morphology was examined using standard techniques of electron microscope fractography in a JEOL scanning electron microscope. An accelerating potential of 25 kV was used to study randomly selected areas.

RESULTS AND DISCUSSION

Fatigue Crack Propagation.

The results of the fatigue crack propagation tests are presented in Figure 3, as a plot of da/dN versus ΔK_1. Tests at a temperature of 20 °C tend to show higher crack growth rates at higher values of ΔK_1 when compared with the tests at 250 °C. At low values of ΔK_1 however, the crack growth rates were observed

to be substantially higher for the tests at 250°C. Fatigue thresholds appear to exist around ΔK_1 =4.3 MN/m$^{3/2}$ and ΔK_1 =2.9 MN/m$^{3/2}$ for temperatures of 20 °C and 250 °C respectively. BALTHAZAR et al [9] show that these values are comparable to several cast irons and equal to or better than other aluminium casting alloys. Although the results overall present a substantial scatter this can be expected for a material tested in the "as cast" condition.

Fracture Morphology.

The general topographical features of the fractured surfaces at various values of da/dN and ΔK_1 at both temperatures used are shown in Figures 4 through 9. Fracture surfaces at 20 °C, in the threshold region (da/dN<10^{-7} mm/cycle), Figure 4, show a mixed mode of ductile tearing, characterized by ridges, in the soft aluminium matrix while the hard silicon precipitate particles were fractured by a cleavage mechanism. The cleavage is well characterized in the facets and in the changing of orientation from one grain to another leading to the crack branching along different planes making, in consequence, the general appearance of the fracture surface very irregular. As tearing is usually observed when small areas remain unbroken behind the main crack front the cleavage of silicon particles, due to their brittle behaviour, seems to be the predominant mechanism of fracture governing crack propagation. This was also observed by PONIEWIERSKI and LINKOWSKI [10] testing a hypoeutectic aluminium-silicon alloy. At 250 °C, the fracture surface in the threshold region, Figure 5, shows the same general behaviour as at 20 °C but with an increased amount of tearing of the soft aluminium matrix. The silicon particles also fractured by cleavage but with changing of fracture planes, give a much less chaotic aspect of the overall fracture surface. At this temperature some traces of microvoid coalescence can also be observed.

Figures 6 and 7, show the fracture surfaces in the Paris regime at 20 °C and 250 °C respectively and a similar overall irregular appearance is observed at both temperatures. The same basic mixed mechanism of cleavage in the silicon particles and ductile fracture by tearing in the soft matrix is maintained but while at 20 °C the ductile fracture in the aluminium matrix occurs almost entirely by tearing, at 250 °C a significant amount of microvoid coalescence can also be observed in several regions as also illustrated in Figure 8, where the cleaved facets are separated by arrays of dimples. However, the degree of flow in such a mechanism does not contribute to ductility and the overall fracture remains brittle in nature. In the Paris regime of crack propagation striations could sometimes be observed, as in Figure 9, where what seems to be a microcrack initiating from an inclusion can also be seen. The striation pattern indicates that the growth of these cracks change from one plane to another as a consequence of more favourable propagation paths. Figures 4,7 and 8 also show the presence of secondary cracks indicating cracking normal to the main fracture plane.

CONCLUSIONS

The fractographic study of fatigue crack threshold and propagation

in the light weight aluminium alloy LM-30 has shown that the silicon precipitate determines the mode of fracture of such an alloy. The fracture mechanism does not change significantly from 20 °C to 250 °C or even from threshold to the Paris regime of crack propagation. The mechanism consists basically of cleavage of the silicon particles ahead of the main crack front leaving behind ligaments of aluminium matrix which fracture in a ductile mode. Tearing was the most frequently observed ductile mechanism but also microvoid coalescence and striations were noted.

SYMBOLS USED

a = crack length.
B = specimen thickness.
K_{max} = maximum stress-intensity.
K_{min} = minimum stress-intensity.
ΔK_1 = stress-intensity range.
N = number of cycles.
ΔP = applied load range.
R = stress ratio.
W = distance between the load axis and the far edge of the specimen.

REFERENCES

[1] - McINTYRE,D.,1975, J. Eng. Mat. Tech. - TRANS. ASME , 97, 194.

[2] - ENGEL,L.,and KLINGELE,H.,1981, An Atlas of Metal Damage , Wolfe Pub., London.

[3] - GERBERICH,W.W.,and MOODY,N.R.,1979, Fatigue Mechanisms , ASTM-STP 675, 292.

[4] - McEVILY,A.J.,1977, Metal Science , 11, 274.

[5] - BEEVERS,C.J.,1977, Metal Science , 11, 362.

[6] - AIME,1979, Metals Handbook , V. 2, 9th ed, USA.

[7] - JORSTAD,J.L.,1968, Trans. Met. Soc. AIME , 242, 1217.

[8] - SAXENA,A.,and HUDDAK Jr,S.J.,1978, J. Fract. Mechanics , 14, 453.

[9] - BALTHAZAR,J.C.,CULVER,L.E.,and RADON,J.C., 1982, Proc. 8th Congress on Material Testing , Budapest,Hungary. To be published.

[10] - PONIEWIERSKI,Z.,and LINKOWSKI,J.,1980, Archiwum Hutnictwa , 25,465.

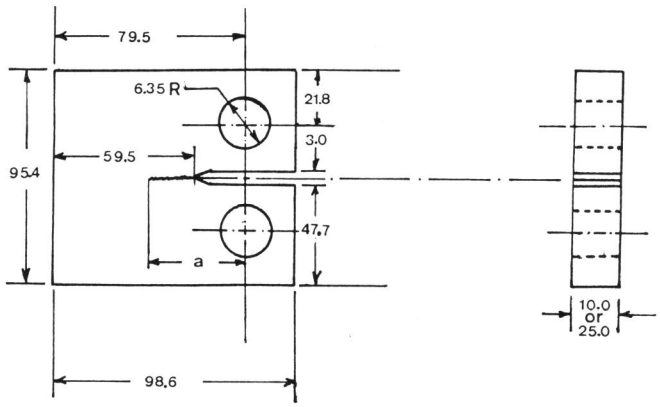

Figure 2 - Compact Specimen.
All dimensions in mm.

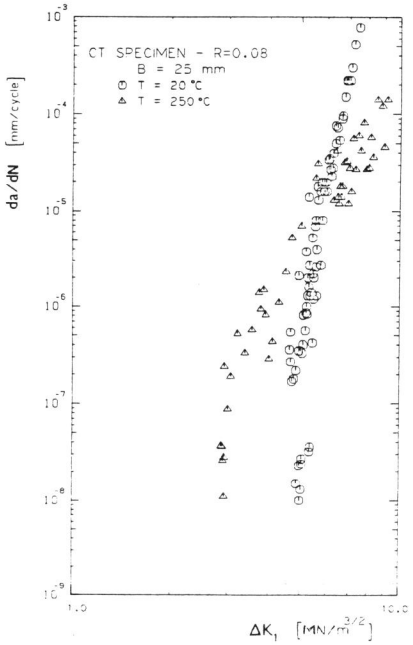

Figure 3 - Temperature Effect on Crack Propagation of LM-30.

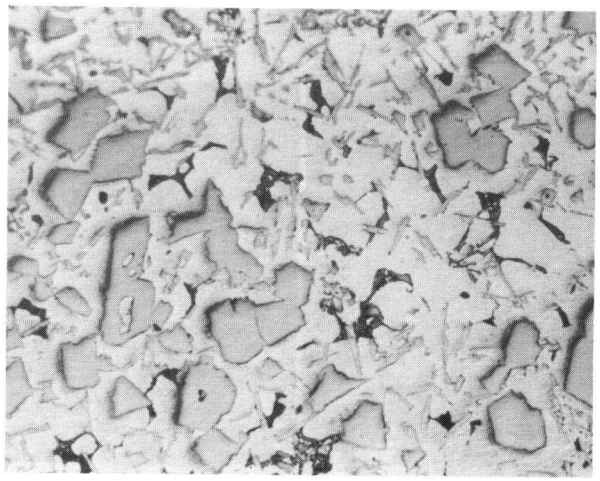

Figure 1 - Microstructure of LM-30.
HF etching. Magnification of 100 times.

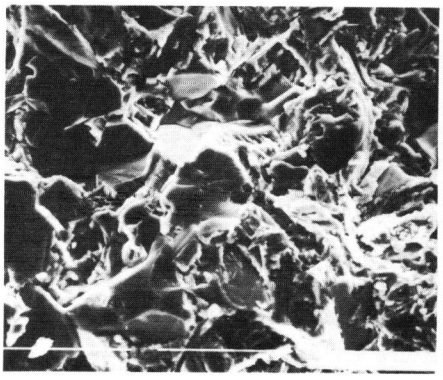

Figure 4 - SEM Photograph of LM-30 Showing Frature Surface in the Threshold Region.
$da/dN < 10^{-7}$ mm/cycle,
$\Delta K_1 \cong 5.0$ MN/$m^{3/2}$,
T = 20 °C, Mag. 350x.

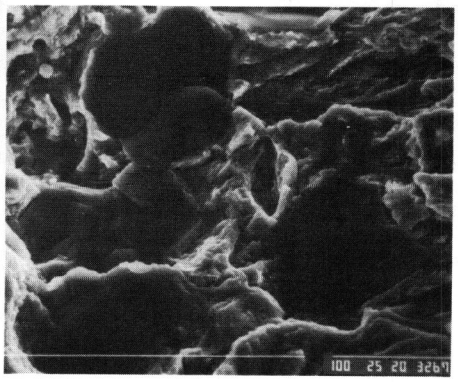

Figure 5 - SEM Photograph of LM-30 Showing Fracture surface in the Threshold Region.
$da/dN < 10^{-7}$ mm/cycle,
$\Delta K_1 \cong 3.0$ MN/$m^{3/2}$,
T = 250 °C, Mag. 750x

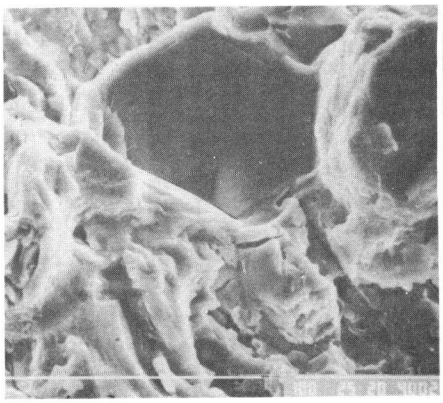

Figure 6 - SEM Photograph of LM-30 Showing Fracture Surface in the Paris Regime.
$da/dN \cong 7 \times 10^{-6}$ mm/cycle,
$\Delta K_I \cong 5.5$ MN/m$^{3/2}$,
T= 20 °C, Mag. 750x.

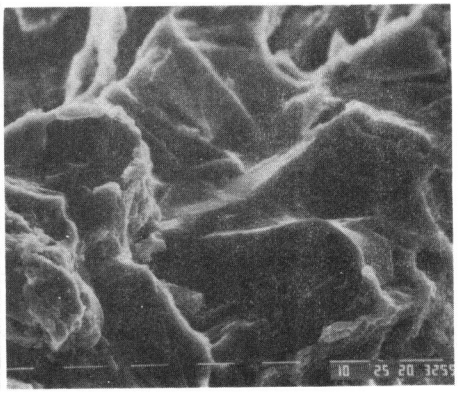

Figure 7 - SEM Photograph of LM-30 Showing Fracture Surface in the Paris Regime.
$da/dN \cong 10^{-5}$ mm/cycle,
$\Delta K_I \cong 4.5$ MN/m$^{3/2}$,
T = 250 °C, Mag. 1000x.

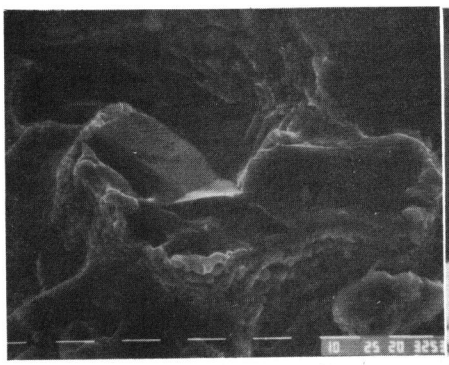

Figure 8 - SEM Photograph of LM-30 Showing Fracture Surface in the Paris Regime.
$da/dN \cong 10^{-5}$ mm/cycle,
$\Delta K_I \cong 4.5$ MN/m$^{3/2}$,
T = 250 °C, Mag. 1000x.

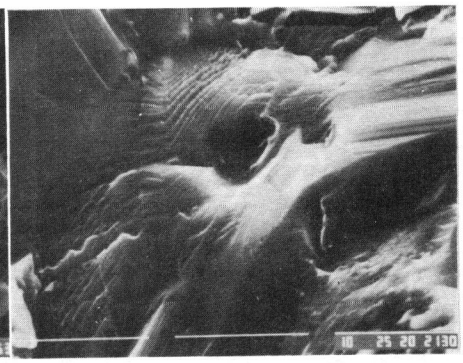

Figure 9 - SEM Photograph of LM-30 Showing Fracture Surface in the Paris Regime.
$da/dN \cong 10^{-4}$ mm/cycle,
$\Delta K_I \cong 6.0$ MN/m$^{3/2}$,
T = 20 °C, Mag. 3500x.